



Highlighting the collaborative research on fuel cell catalysts
by Prof. Mitsuharu Chisaka at Hirosaki University and
Dr. Hiroyuki Morioka at Toppan Printing Co., Ltd.

Phosphor and nitrogen co-doped rutile TiO_2 covered on TiN for oxygen reduction reaction in acidic media

A new oxygen reduction reaction catalyst, phosphor and nitrogen co-doped rutile TiO_2 was synthesized on TiN without carbon supports. Pentavalent phosphor doping enhanced the mass activity by more than double to create novel active sites.

As featured in:



See Mitsuharu Chisaka and
Hiroyuki Morioka,
Catal. Sci. Technol., 2019, 9, 611.



Cite this: *Catal. Sci. Technol.*, 2019,
9, 611

Received 22nd September 2018,
Accepted 29th November 2018

DOI: 10.1039/c8cy01973h

rsc.li/catalysis

Phosphor and nitrogen co-doped rutile TiO_2 covered on TiN for oxygen reduction reaction in acidic media[†]

Mitsuharu Chisaka ^{*a} and Hiroyuki Morioka^b

Phosphor and nitrogen atoms were simultaneously doped into rutile TiO_2 covered on TiN for oxygen reduction reaction in acidic media, without using carbon supports. A recently reported facile combustion method was modified by simply adding H_3PO_4 to the precursor dispersion. Pentavalent phosphor (P^{5+}) atoms were doped into both the bulk and surface to form new active sites without altering the number of oxygen vacancies on the rutile surface, which was formed by nitrogen doping. The P^{5+} -doping successfully enhanced the ORR mass activity by more than double. However, the activity was not stable after 5000 potential cycles between 1.0 and 1.5 V versus reversible hydrogen electrode, due to the partial loss of both phosphor and nitrogen atoms. The stabilization of these foreign atoms at high potential was revealed to be necessary to use this catalyst without incurring costly potential protection systems.

1. Introduction

Rechargeable batteries and polymer electrolyte fuel cells (PEFCs) have received an increasing attention in recent years to replace the conventional internal combustion vehicle engines, owing to the worldwide trend in regulating the vehicle emissions. These two electrochemical devices, as the vehicle power source, excel at different driving range and load because of the difference in operating principles, *i.e.*, energy storage and energy conversion. For increasing the driving range or load of battery-driven electric vehicles (EVs) to store the energy, the mass, volume and resulting cost of rechargeable batteries should increase. In contrast, the mass and/or volume of only hydrogen tank should increase to increase the driving range of PEFC-powered vehicles (FCVs). For mid-size passenger vehicles, 200–300 miles of driving range has been considered to be the criteria to select one from these two technologies and above 300 miles, only FCVs will be available.^{1–3} Besides, FCVs are also suitable for carrying high loads of buses and trucks compared with EVs.³ Despite the technical advantages of PEFCs, the widespread use of FCVs has not yet been recorded. Even if worldwide hydrogen infrastructures were built from green renewable energies at accept-

able costs, current usage of platinum-group-metal (PGM) catalysts at PEFC cathodes would be too high for the mass production. At PEFC cathodes in the current commercial FCVs, carbon-supported platinum-cobalt alloy is used to catalyse oxygen reduction reaction (ORR).⁴ Owing to the slow kinetics of ORR, currently *ca.* 4 times larger amount of PGM is needed at the cathode compared with the anode counterpart,⁵ which also utilizes platinum to catalyse hydrogen oxidation reaction (HOR). Thus, most of PGM in the FCVs is still platinum. When achieving the 2020 target set by U.S. Department of Energy (DOE), *i.e.*, 0.125 g of PGM per kilowatt,⁶ 14 g of PGM is still required for a 114 kW-class sedan, such as MIRAI from Toyota Mortars.⁴ The world production of platinum in 2017 was 20 000 kilograms,⁷ and therefore, only 1.4 million FCVs can be produced even if all the produced platinum was used up for the passenger vehicles. This value, 1.4 million, is less than 2% of the annual production of the passenger vehicles in 2017, which was 73.5 million.⁸ Therefore, the scarce resource of platinum catalyst is the barrier for the widespread use of automotive PEFC.

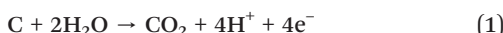
Earth abundant cathode catalysts free from PGM have therefore been of particular interest. The cathode catalysts are under highly oxidative conditions, as (i) they are in contact with proton conductive perfluorosulfonate ionomer, such as Nafion in the catalyst layer, and (ii) the operating potential in FCVs is between 0.6 and 1.0 V versus the reversible hydrogen electrode (RHE). Only one type of non-PGM catalyst, the so-called Fe/N/C, has shown promising initial activity and most researchers in non-PGM catalyst community have focused on this catalyst type. Particularly after the performance

^a Department of Sustainable Energy, Hirosaki University, 3 Bunkyo-cho, Hirosaki, Aomori 036-8561, Japan. E-mail: chisaka@hirosaki-u.ac.jp

^b Technical Research Institute, Tappan Printing Co., Ltd, 4-2-3 Takanodaiminami, Sugito-machi, Saitama 345-8508, Japan

[†] Electronic supplementary information (ESI) available: Experimental details, XRD patterns, XPS depth profiles, Nyquist plots, FE-SEM images, ORR activity and selectivity data. See DOI: 10.1039/c8cy01973h

breakthrough with the use of metal organic framework precursor by Dodelet *et al.* in 2011,⁹ highly active Fe/N/C catalysts whose performance is comparable to that of commercial carbon-supported platinum have been reported by other groups.¹⁰ Major part of the Fe/N/C catalyst volume was occupied by nitrogen-doped graphitic carbon species, whereas the high activity was always delivered by introducing iron atoms.^{9–11} Other non-PGM catalyst type, oxide/oxynitride-containing group IV or V metals have attracted less attention compared with Fe/N/C in this field.¹² The advantage of this catalyst type is the chemical stability preventing leaching in acidic media,¹³ whereas the disadvantages are the moderate activity and low conductivity. In 2017, we reported the highest activity among oxide/oxynitride-based catalysts from zirconium oxynitride supported on a multi-walled carbon nanotube (ZrO_xN_y -MWCNT). The single-cell performance was comparable to that of state-of-the-art Fe/N/C catalysts¹⁴ to attract the attention of pioneers of Fe/N/C.¹¹ However, the performance was not stable even when the cell voltage was maintained below 1 V.¹⁴ Carbon species are known to be oxidised to form carbon dioxide in the presence of water at above 0.207 V *versus* the standard hydrogen electrode:



The rate of graphitic carbon species in eqn (1) is generally low and the degradation of typical carbon black, Vulcan XC-72R, initiates at ~1.1 V.¹⁵ However, when platinum particles were supported on the Vulcan XC-72R, they catalysed (1) at a much lower potential, ~0.5 V.¹⁵ The defective carbon species in Fe/N/C were oxidised below 0.7 V.¹¹ One of the reasons for the abovementioned ZrO_xN_y -MWCNT degradation could be the oxidation of carbon species that originated from the zirconium oxypythalocyanine precursor and MWCNT.

We have recently shifted our focus to another group IV metal oxynitride catalyst, namely titanium oxynitride (TiO_xN_y). It was originally synthesised on carbon black,¹⁶ whereas much better activity was obtained by replacing the carbon black with Ti_4O_7 fibre¹⁷ and the best one was from support-free TiO_xN_y catalysts.^{18,19} The bulk of the catalyst was metallic nitride, TiN, and recent analyses revealed that both the activity and conductivity originated from the oxidised TiN surface, TiO_xN_y , and not the carbon residues from urea precursor.¹⁸ Although TiN is well known to be electronically conductive, the conductivity of the active oxidised surface should be lower than the bulk TiN. Therefore, the enhancement of the surface conductivity can improve the ORR activity.

As electron donors, pentavalent transition metals such as niobium²⁰ and tantalum²¹ have been used to substitute tetravalent titanium atoms in TiO_2 for enhancing conductivity. Compared with these metals, the non-metal phosphor is far more abundant and inexpensive; even human urine has been used as a phosphor source of P^{5+} -doped anatase TiO_2 .²² The electron conductivity enhancement of anatase TiO_2 by P^{5+} -doping has also been reported.²³ Thus, pentavalent phosphor doping is a potential economic and attractive pathway to in-

crease the activity of our TiO_xN_y ORR catalyst whose surface was amorphous or rutile TiO_2 ,^{17–19} different from the previous reports on anatase counterpart.^{22,23}

In this study, a new ORR catalyst, phosphor and nitrogen co-doped rutile TiO_2 on TiN, hereafter denoted as $TiO_xN_yP_z$ for simplicity, was synthesised. Phosphor doping was revealed to successfully enhance the activity of TiO_xN_y for the first time.

2. Experimental section

The $TiO_xN_yP_z$ catalysts were synthesised by modifying a recently reported facile combustion method^{16–19} without using supports. The detailed catalyst synthesis and characterisation methods are described in S1, ESI.† Titanium oxsulfate powder and H_3PO_4 solution were first mixed for 2 h. Subsequently, urea powder and HCl solution were added at room temperature. The mass ratio of urea to titanium oxsulfate-derived TiO_2 was set at 100 unless otherwise noted and the HCl concentration in the precursor dispersion was set at 1.0 mol dm⁻³. The atomic ratio of phosphor to titanium, R_P , was varied from 0.0 to 1.0. The dispersion was then heated with continuous mixing, followed by drying. The dried powders were pyrolysed at 1123 K for 2 h under flow of N_2 gas. Some catalysts were further annealed under flow of NH_3 gas at different temperatures and for different durations.

The bulk and surface crystal structures of catalysts were investigated by analysing X-ray diffraction (XRD) patterns and Raman spectra, respectively. The chemical states of the catalysts were determined by X-ray photoelectron spectroscopy (XPS). For some catalysts, the surface was sputtered with an Ar^+ -ion beam generated at an acceleration voltage of 500 V or 1 kV for 60 s. The spectra were recorded after the sputtering and the procedure was repeated for five times. The peak shifts due to surface charge were corrected using the binding energy of C 1s (284.8 eV), which originated from the spectrometer hydrocarbon contaminants. The morphology of the $TiO_xN_yP_z$ catalysts was investigated using the field emission scanning electron microscopy (FE-SEM) and transmission electron microscopy (TEM) images.

Rotating disk electrode (RDE) and rotating ring-disk electrode (RRDE) voltammograms were obtained to evaluate the ORR activity and selectivity, respectively, of the catalysts. The mass fraction of Nafion in the catalyst layer was set at 0.05 and the catalyst loading, m , was varied from 0.6 to 1.5 mg cm⁻². A conventional three-electrode cell was used for the room-temperature electrochemical measurements performed in 0.1 mol dm⁻³ H_2SO_4 . After sequentially bubbling O_2 and N_2 for 1800 s, RDE and RRDE voltammograms were recorded by applying a disk potential (E) of 0.05–1.2 V *versus* the reversible hydrogen electrode (RHE) at a scan rate of 5 mV s⁻¹ and a rotation speed of 1500 rpm. The ring potential was maintained at 1.2 V to obtain RRDE voltammograms that were used to calculate the hydrogen peroxide yield, $X_{H_2O_2}$. The ORR was measured by $j = j_O - j_N$, the difference between the

current per unit geometrical area, S , of the disk electrode obtained in N_2 ($j_{\text{N}} = I_{\text{N}} S^{-1}$) and in O_2 ($j_{\text{O}} = I_{\text{O}} S^{-1}$).

3. Results and discussion

The catalysts were synthesised using five different R_{P} and the effect on the crystal structure in bulk (XRD pattern) and surface (Raman spectra) are shown in Fig. 1(A) and (B), respectively. All the $\text{TiO}_{x}\text{N}_y\text{P}_z$ catalysts showed a single TiN phase and no peaks from phosphorous compounds such as TiP_2O_7 and P_3N_5 appeared even at the highest R_{P} of 1.0 as shown in Fig. 1(A), which indicate that phosphorous species from H_3PO_4 precursor did not segregate to form the abovementioned crystalline species during the first pyrolysis at 1123 K. Besides, the peaks did not broaden, and thus, the crystallite size of TiN did not decrease with the increasing R_{P} . In some applications, phosphor doping has been used to reduce the size of various nanomaterials to enlarge the surface area; anatase TiO_2 for photocatalysts,^{24–26} platinum-ruthenium (PtRu) nanoparticles for direct methanol fuel cell anode catalysts²⁷ and iron single crystals in an alumite film for magnetic recording media.²⁸ However, a decrease in crystallite size and the resulting anatase TiO_2 particle size reduction by phosphor doping was reported when the reaction temperature was below 973 K.^{24,25} The phosphor doping into PtRu nanoparticles and iron crystals was performed without annealing to observe the size reduction.^{27,28} From the systematic study by Li *et al.*, the crystallite size of anatase did not change with phosphor-doping when the temperature was higher than 973 K.²⁶ In this study, the pyrolysis temperature of 1123 K and the huge amount of reactive gases evolved during the pyrolysis to produce TiN, mainly from NH_4Cl (S_2 ,

ESI^{\dagger}), could be the reasons for the independency of the crystallite size on R_{P} .

Although the bulk crystal structure of the $\text{TiO}_{x}\text{N}_y\text{P}_z$ catalysts was revealed to TiN, the surface was different. Fig. 1(B)-i displays the Raman spectra of commercial rutile TiO_2 powders (dashed curve) and phosphor-free TiO_{x}N_y catalyst ($R_{\text{P}} = 0.0$, solid curve). The former showed two peaks at ~ 443 and $\sim 606 \text{ cm}^{-1}$, assigned to E_g and A_{1g} vibration modes of stoichiometric rutile TiO_2 , respectively,^{29,30} whereas the E_g peak of the latter shifted to lower wave number region, which indicate that oxygen vacancies were incorporated into the surface rutile TiO_2 by nitrogen doping.^{19,29,31} The TiO_{x}N_y displayed broader peaks compared with commercial rutile, which also indicates the oxygen vacancy incorporation.³⁰ As shown in Fig. 1(B)-ii-v, the defective, oxygen vacancy-incorporated rutile phase was retained after increasing R_{P} because of the appearance of no new peaks and no peak shifts in these $\text{TiO}_{x}\text{N}_y\text{P}_z$ catalyst series. The results of XRD patterns and Raman spectra indicate that nitrogen-doping produced oxygen vacancy on the surface of rutile TiO_2 phase covered on TiN-core, which are in good agreement with our previous studies,^{16–19} whereas phosphor doping did not change the crystal structure both in bulk and on the surface.

The surface chemical states of these $\text{TiO}_{x}\text{N}_y\text{P}_z$ catalyst series were investigated using XPS, and the $\text{Ti} 2p$, $\text{O} 1s$, $\text{N} 1s$ and $\text{P} 2p$ spectra are shown in Fig. 2. The $\text{Ti} 2p$ level splits into the $\text{Ti} 2p_{3/2}$ and $2p_{1/2}$ sublevels *via* spin-orbit coupling to display doublets in the spectra.

Before phosphor doping, the main peak was at $\sim 458.3 \text{ eV}$ in $\text{Ti} 2p_{3/2}$ region as shown in Fig. 2(i), indicating that the valency of the surface Ti was mostly $4+$.^{32,33} Therefore, the surface of TiN was oxidised to agree with the results from the XRD and Raman analyses. The shoulder peak at 456–457 eV

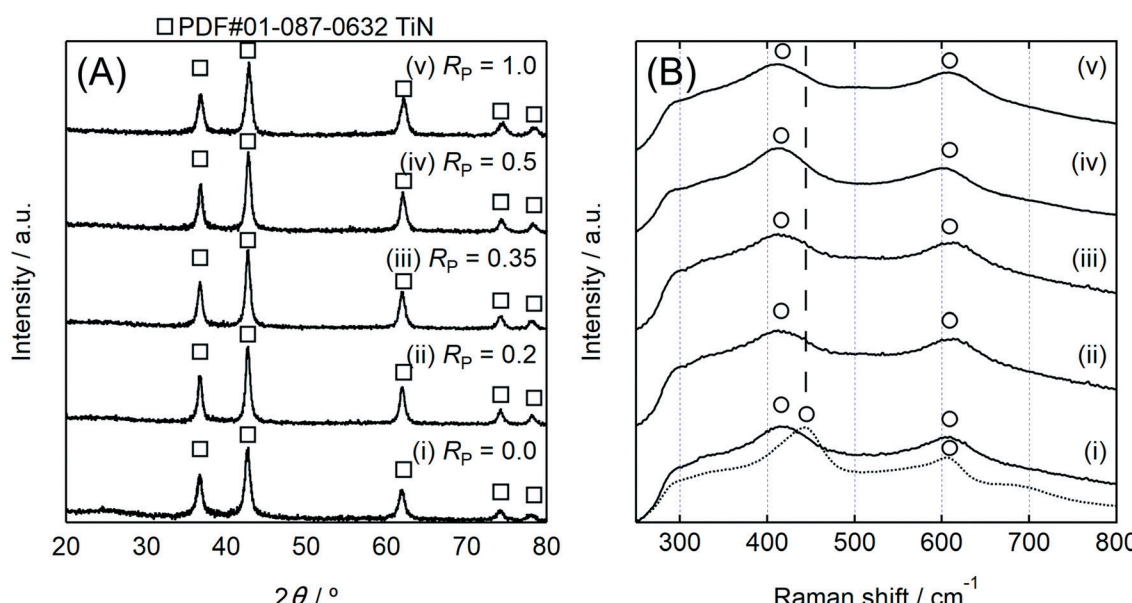


Fig. 1 (A) X-ray diffraction (XRD) patterns and (B) Raman spectra of $\text{TiO}_{x}\text{N}_y\text{P}_z$ catalysts with five different phosphor-to-titanium atomic ratios, R_{P} , (i) 0.0, (ii) 0.2, (iii) 0.35, (iv) 0.5 and (v) 1.0 after N_2 -pyrolysis at 1123 K for 2 h. For reference, a Raman spectrum of commercial rutile TiO_2 powders is shown by a dashed curve in (B).

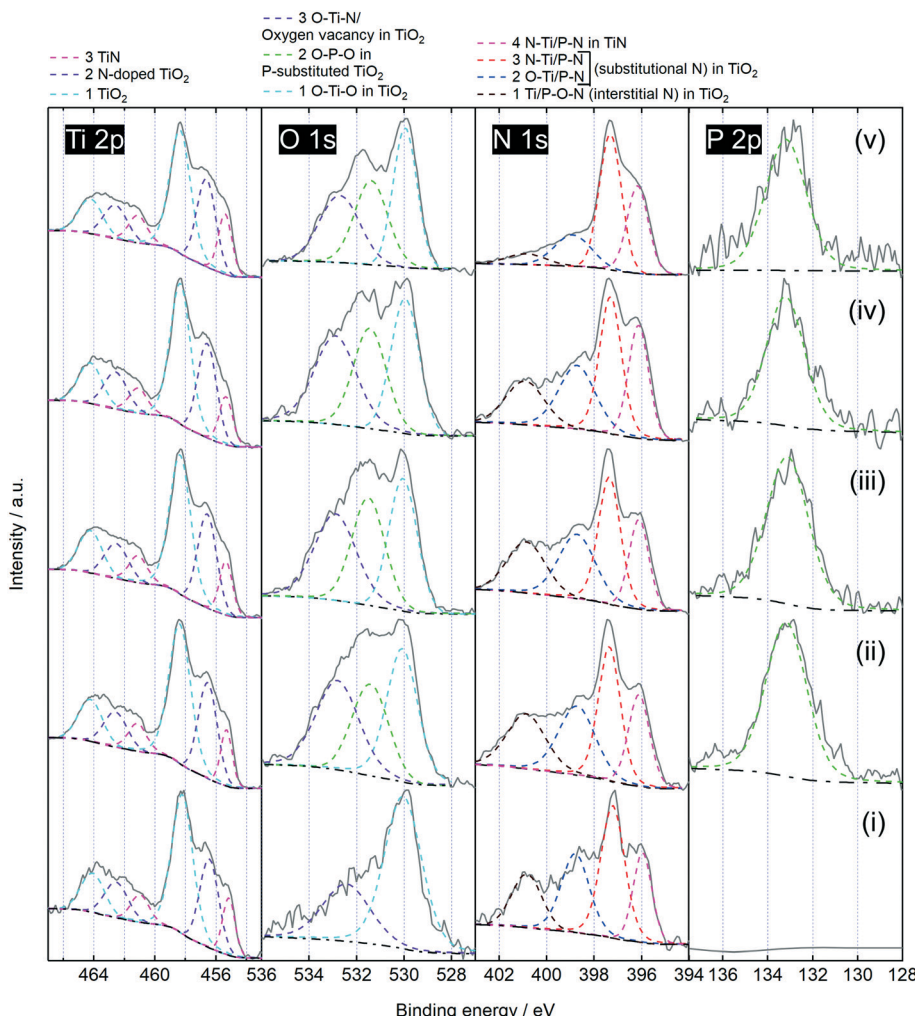


Fig. 2 X-ray photoelectron (XP) Ti 2p, O 1s, N 1s and P 2p spectra of $\text{TiO}_x\text{N}_y\text{P}_z$ catalysts with five different R_{P} , (i) 0.0, (ii) 0.2, (iii) 0.35, (iv) 0.5 and (v) 1.0 after N_2 -pyrolysis at 1123 K for 2 h. The spectra (solid curves) are shown with deconvolution into several peaks (dashed line) after subtracting a Shirley-type background (dash-dotted line).

indicates the formation of TiO_xN_y ^{32,33} and most nitrogen atoms substituted lattice oxygen in TiO_2 , as evidenced by ~397 and ~399 eV peaks in the N 1s spectrum.^{17–19,34} The formation of substitutional nitrogen-doped TiO_2 phase was also confirmed from the corresponding O 1s spectrum displayed in Fig. 2(i). The main peak at ~530 eV is assigned to lattice oxygen in TiO_2 (ref. 33 and 35) and the shoulder one at ~532 eV is oxygen vacancy in TiO_2 lattice³⁵ formed by substitutional nitrogen doping (O-Ti-N bonding).³³

Fig. 2(ii) shows that both the Ti 2p and N 1s spectra did not change significantly after phosphor doping at $R_{\text{P}} = 0.2$, whereas a peak at ~531 eV appeared in the O 1s spectrum, which is assigned to O-P-O bonding in phosphor-doped TiO_2 .³⁶ Simultaneously, a peak at ~133 eV appeared in the P 2p spectrum, which has been assigned to cationic P^{5+} that substituted titanium atom in phosphor-doped TiO_2 (ref. 22–25) and in phosphor and nitrogen co-doped TiO_2 .^{36,37} These results indicate that phosphor atoms substituted titanium atoms on the surface TiO_2 lattice. There was no anionic

P^{3-} peak at ~129 eV,^{23,38} indicating that the surface was free from Ti-P bonds. The valency of the phosphor atoms in the sub-surface was investigated using Ar^+ -ion beam sputtering with two different acceleration voltages, 500 V and 1 kV. After sputtering the surface with Ar^+ ion beam at the lower acceleration voltage, 500 V up to 5 minutes, the P 2p spectra were still free from P^{3-} peaks, whereas the TiN peak at ~455 eV (ref. 32 and 33) in Ti 2p spectra grew up with the increasing sputtering time (S3, ESI†). The trend did not change at the deeper part in the bulk, as displayed by increasing the acceleration voltage of sputtering to 1 kV (S3, ESI†). These results indicate that most P^{5+} formed solid solutions with both bulk TiN and surface rutile TiO_2 . The valency of surface titanium was mostly 4+, and the chemical states of both titanium and nitrogen did not change with phosphor doping from Fig. 2(i) and (ii) and the deconvolution results summarized in Fig. 3. The number of oxygen vacancy did not change too from their Raman spectra displayed in Fig. 1(B)-i and ii. The area fraction of the peak from oxygen vacancy at ~532 eV in

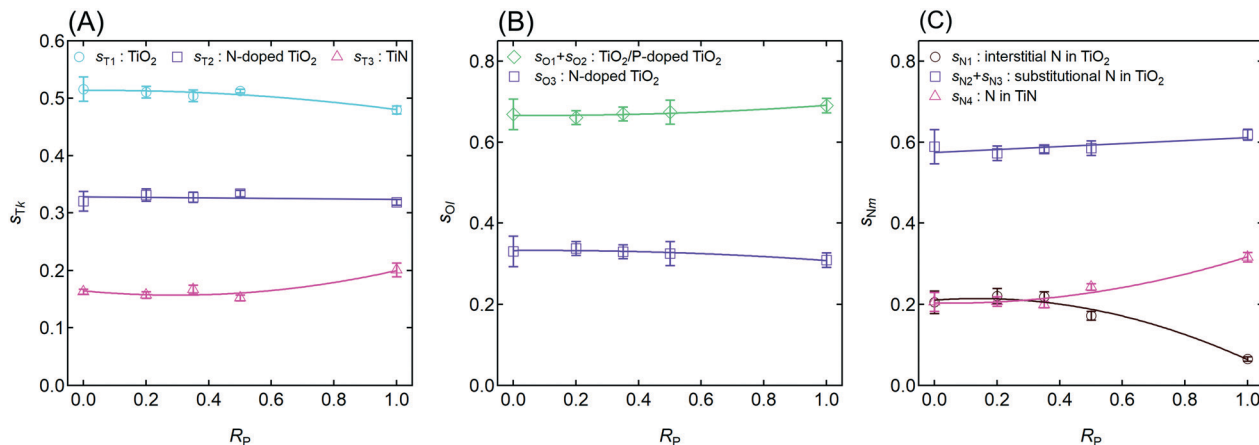


Fig. 3 Area fractions of (A) three pairs of doublets in Ti 2p region, (B) three peaks in O 1s region and (C) four peaks in N 1s region versus the phosphor-to-titanium atomic ratio ($s_{T_K} - R_P$, $s_{O_I} - R_P$ and $s_{N_m} - R_P$ curves, respectively) calculated from Fig. 2.

their O 1s spectra, s_{O_3} , did not change as shown in Fig. 3(B), which is in good agreement with the trend from the Raman spectra. The charge imbalance due to the doped P⁵⁺ should therefore be compensated by titanium vacancy. The spectra remained almost the same, and thus, the area fraction of each peaks did not change with increasing R_P to 0.5 as shown in Fig. 2(ii)–(iv) and Fig. 3, respectively. However, in Ti 2p region, the area fraction of the peak from TiN, s_{T_3} , increased and that from TiO₂, s_{T_1} , decreased when R_P was further increased to 1.0 as shown in Fig. 2(v) and 3(A). The trend agrees well with that from N 1s region, which is summarized in Fig. 3(C); the area fraction of TiN, s_{N_4} , increased, whereas that of interstitial nitrogen in TiO₂, s_{N_1} , decreased with increasing R_P from 0.5 to 1.0. At $R_P = 1.0$, the byproducts attached much more severely to the inner wall of the quartz tube at the heating zone after pyrolysis than those at $R_P \leq 0.5$ (S1, ESI†). These results indicate that, during the mixing and pyrolysis processes, excess H₃PO₄ reacted with other pre-

cursors to change the chemical states of TiO_xN_yP_z. The content of interstitial nitrogen in the TiO₂ lattice, which was less stable compared with substitutional nitrogen, decreased. As a result of the decrease in s_{N_1} , s_{N_4} became larger at $R_P = 1.0$.

In contrast to the similarity of the crystal structures (Fig. 1) and chemical states (Fig. 2 and 3), the ORR activity of these catalysts significantly depended on R_P , as shown in Fig. 4(I). The activity increased drastically when R_P was increased from 0.0 to 0.2, indicating the formation of new active sites by phosphor doping. The results from Fig. 1(i)–(ii) indicated that both these catalysts were rutile TiO₂ covered on TiN and the number of oxygen vacancies on the surface rutile, which has been revealed to be necessary for the formation of ORR active sites on phosphor-free TiO_xN_y¹⁹ was similar. The chemical states of titanium and nitrogen were also similar at $0.0 \leq R_P \leq 0.2$ and the sole difference was the presence of P⁵⁺ as shown in Fig. 2(i) and (ii). These results suggest that (1) doped P⁵⁺ itself and/or (2)

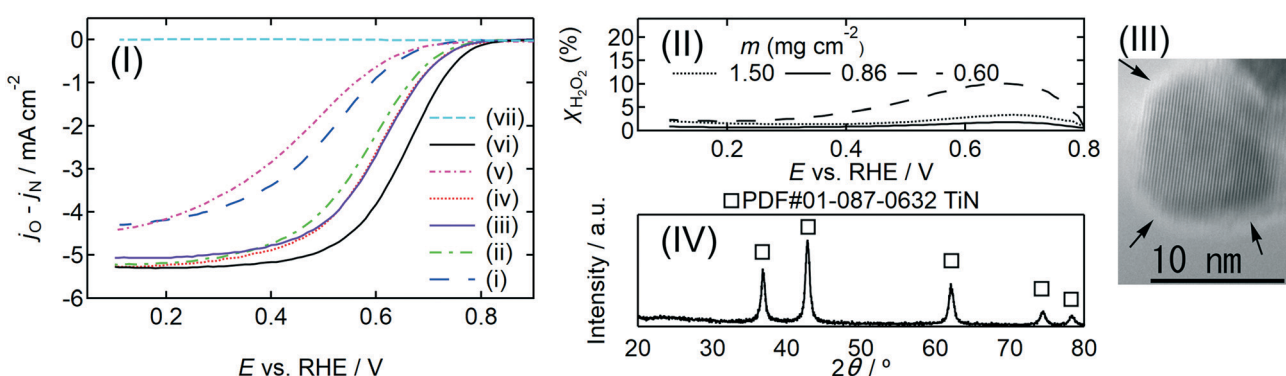


Fig. 4 (I) Rotating disk electrode (RDE) voltammograms of TiO_xN_yP_z catalysts with five different R_P , (i) 0.0, (ii) 0.2, (iii) 0.35, (iv) 0.5 and (v) 1.0 after pyrolysis under flow of N₂ gas at 1123 K for 2 h and of (vi) $R_P = 0.35$ sample after the second annealing under flow of NH₃ gas at 923 K for 3 h. As a reference, a RDE voltammogram of (vii) TiO₂ powders after NH₃ annealing at 1123 K for 3 h is also shown. The scans were performed in N₂ and O₂ atmospheres, at a rotation speed of 1500 rpm and a scan rate of -5 mV s⁻¹ (cathodic) in 0.1 mol dm⁻³ H₂SO₄. The m of TiO_xN_yP_z catalysts was set constant at 0.86 mg cm⁻² except for (i), 1.00 mg cm⁻². The m of NH₃-annealed TiO₂ was 2.00 mg cm⁻². (II) Hydrogen peroxide yield versus potential ($X_{H_2O_2}$ – E) curves with three different m . (III) A high-resolution transmission electron microscopy (HR-TEM) image and (IV) a XRD pattern of (vi).

titanium vacancy created by P⁵⁺-doping to compensate the charge imbalance formed new active sites for ORR. Titanium vacancy on the surface of rutile (110) plane is known to be a dissociative adsorption site for an O₂ molecule,³⁹ which should be the first step for ORR. Besides, a titanium vacancy traps up to four protons to form the so-called Ruetschi defects,^{40,41} similar to the manganese defects in MnO₂.⁴² Thus, surface proton conductivity is expected to be enhanced by the incorporation of titanium vacancies.⁴⁰ Coexistence of oxygen vacancy and titanium vacancy on TiO₂ has also recently been reported to enhance the surface electron conductivity, leading to an improvement in lithium/sodium ion battery performances.⁴¹ Although the precise mechanism for the ORR activity enhancement displayed in Fig. 4(I)-i and ii is not clear at this stage, substitutional P⁵⁺ doping into TiO₂ lattice should induce at least abovementioned several factors, *i.e.*, creation of the dissociative adsorption sites for O₂ molecule, proton/electron conductivity enhancement. All these factors could enhance the ORR activity, and the dominant process should be clarified in the future study by, for example, density functional theory calculations. Besides, surface phosphate ions have recently been reported to enhance the electron conductivity and reaction kinetics of cobalt oxide pseudo capacitors.⁴³ Similar effect on the present TiO_xN_yP_z catalysts can be expected from the Nyquist plots (S4, ESI†). The ORR activity remained almost constant when R_P was increased up to 0.5, which is in good agreement with the similarity in the crystal structure and chemical states shown in Fig. 1(ii)–(iv) and 2(ii)–(iv), respectively. However, further increasing R_P to 1.0 decreased the activity significantly as shown in Fig. 4(I)-v. This result was caused by two factors: the changes in the surface chemical states and the active surface area. When R_P was increased from 0.5 to 1.0, the content of surface TiN increased as seen in the analyses of XP spectra shown in Fig. 2 and 3. In our previous studies on phosphor-free TiO_xN_y catalysts, the ORR activity decreased with the increase in s_{T3} to 0.19, as the surface TiN was not stable in acidic media, and it should be covered by oxynitride.¹⁶ The TiO_xN_y catalysts exhibited best performance at s_{T3} < 0.19.¹⁸ Similarly, the activity of TiO_xN_yP_z catalyst in the present study deteriorated at R_P = 1.0 owing to high s_{T3}, 0.20. Although the reason is not clear, the catalysts agglomerated at the highest R_P of 1.0 (S5, ESI†) to decrease the sample volume. Besides, too many phosphate ions have been reported to adsorb strongly on the surface of TiO₂ and reduce the rate of photocatalytic oxidation for organic compounds such as salicylic acid, aniline and ethanol.⁴⁴ Therefore, the active surface area of TiO_xN_yP_z at R_P = 1.0 was too low to decrease the activity. Commercial TiO₂ powders were annealed under NH₃ gas at a temperature identical to that of the first pyrolysis for TiO_xN_yP_z, 1123 K, whereas much lower activity was obtained as shown in Fig. 4(I)-vii, which manifests the superiority of the present synthesis route. The TiO_xN_yP_z catalyst that displayed the highest activity level, for the sample at R_P = 0.35, was further annealed under flow of NH₃ gas. After systematically optimising the NH₃-annealing temperature and

duration (S6, ESI†), the activity was successfully enhanced to shift the curve positively by 0.08 V at m = 0.86 mg cm⁻², which is less than half of our previous carbon-support-free TiO_xN_y catalysts^{17–19} and even 40% lower than that of the best oxide/oxynitride-based catalyst with carbon supports, ZrO_xN_y-MWCNT,¹⁴ to outperform the mass activity (S7, ESI†). The reaction mechanism was close to a four-electron reaction in which an oxygen molecule is directly reduced to water (O₂ + 4H⁺ + 4e⁻ → 2H₂O), to display less than 5% of X_{H₂O₂} formed by a 2-electron reaction (O₂ + 2H⁺ + 2e⁻ → H₂O₂) as shown in Fig. 4(II). However, the X_{H₂O₂} value increased when m was reduced to 0.60 mg cm⁻², which indicates that at higher m, some hydrogen peroxide molecules formed at the bottom of the catalyst layer near glassy carbon electrode side were further reduced to water before passing through the thicker catalyst layer *via* an electrochemical path (H₂O₂ + 2H⁺ + 2e⁻ → 2H₂O) or a chemical decomposition (H₂O₂ → H₂O + 0.5O₂). The morphology of the NH₃-annealed sample was further investigated by HR-TEM, and the image is displayed in Fig. 4(III). A crystallized inner particle showed clear lattice fringes and a disordered outer layer covered on it as indicated by arrows, similar to previously reported hydrogenated TiO₂ in which disordered outer layer covered crystalline anatase inner core.⁴⁵ Therefore, the outer surface contained some defects. The grain size of the sample was calculated to be 13.7 nm from the XRD pattern shown in Fig. 4(IV). This value is slightly higher than that before NH₃-annealing calculated from the XRD pattern shown in Fig. 1(A)-iii, 12.6 nm, which indicates that aggregation during the NH₃ annealing was not severe, as the annealing temperature, 923 K, was lower than the temperature in the initial pyrolysis process under flow of N₂ gas, 1123 K.

Durability of TiO_xN_yP_z, which showed the highest activity level, was investigated using a start-up/shut-down protocol for automotive PEFC proposed by Fuel Cell Commercialisation Conference of Japan (FCCJ),⁴⁶ in which the E was cycled between 1.0 and 1.5 V. During the start-up and shut-down of the cell, anode reacts with oxygen from air, which is catalysed to water by the anode platinum catalysts. Thus, the counter cathode potential increases up to ~1.4 V by the so-called reverse-current decay mechanism,⁴⁷ to accelerate the corrosion of carbon supports under platinum-cobalt catalysts by increasing the rate in eqn (1). The cathode potential is therefore currently controlled below 1 V by system-level measures, *i.e.*, reducing the air flow rate in the cathode at the shutdown to minimize oxygen diffusion to the anode through membrane and flowing the extra hydrogen gas to the anode after the shutdown to consume oxygen gas chemically for preventing the anode ORR.⁴⁸ These measures, in turn, increase the cost of PEFC system, and thus, TiO_xN_yP_z catalysts can reduce the cost if they were tolerant to the high potential cycling. Fig. 5 and 6 displays the RDE voltammograms and the XP spectra of the TiO_xN_yP_z catalyst before/after 5000 cycles, respectively. The RDE voltammogram shifted negatively by 0.11 V after 5000 cycles, as shown in Fig. 5. The cycles decreased the area fractions of peak at ~457 and ~397 eV of the Ti 2p_{3/2} and N 1s spectra,

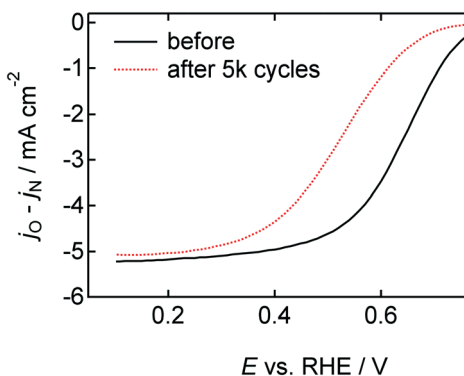


Fig. 5 RDE voltammograms of $\text{TiO}_x\text{N}_y\text{P}_z$ ($R_p = 0.5$) catalyst before (solid curve) and after (dashed curve) 5000 potential cycles between 1.0 and 1.5 V vs. RHE at 0.5 V s^{-1} in 0.1 mol dm^{-3} H_2SO_4 solution. Before and after 5000 cycles, the scans were performed in N_2 and O_2 atmospheres, at a rotation speed of 1500 rpm and a scan rate of -5 mV s^{-1} (cathodic) for evaluating the activity. The catalyst was synthesised via two-step heating processes: the first under flow of N_2 at 1123 K for 2 h followed by the second under NH_3 flow at 873 K for 3 h.

respectively, as shown in Fig. 6, which indicates the removal of surface nitrogen atoms that substituted oxygen atoms in rutile TiO_2 lattice. Furthermore, those at ~ 455 and ~ 395 eV also decreased after 5000 cycles shown in Fig. 6, as surface TiN was removed by the cycles. The removal of P^{5+} was also indicated from the $\text{P} 2p$ spectra in Fig. 6. These results indicate that phosphor and nitrogen co-doping into the surface rutile TiO_2 phase on TiN is effective for enhancing the ORR activity, whereas the doped foreign atoms are not stable against the high potential cycling. Although the degradation mechanism of Fe/N/C catalyst has been debated extensively,^{11,49} no discussion has been carried out for the oxide/oxynitride catalysts. For the first time, the present study revealed that stabilization of these foreign atoms in the lattice is necessary to utilize this catalyst without keeping the potential below 1.0 V, which is commonly adopted in the PEFCs operation to increase the system cost.

Chen *et al.*⁵⁰ reported that nitrogen atoms in TiO_2 lattice were stabilized by simply annealing the nitrogen-doped TiO_2 in air at low temperature for improving the stability of photocatalytic ethylene oxidation reaction. In that study, the annealing also reduced the number of surface oxygen vacancies,⁵⁰ which should be unfavourable for ORR.¹⁹ One possible way to stabilize foreign atoms in the TiO_2 lattice of the present catalysts is to perform such post annealing under optimized conditions not to lose vacancies by using, for example, reductive atmosphere. Another way to improve the stability could be the use of a new two-dimensional support,⁵¹ which has recently been reported to show strong interactions with TiO_2 photocatalysts for the degradation of methylene blue.⁵²

Conclusions

Phosphor and nitrogen atoms were co-doped into rutile TiO_2 phase formed on TiN without carbon supports to ca-

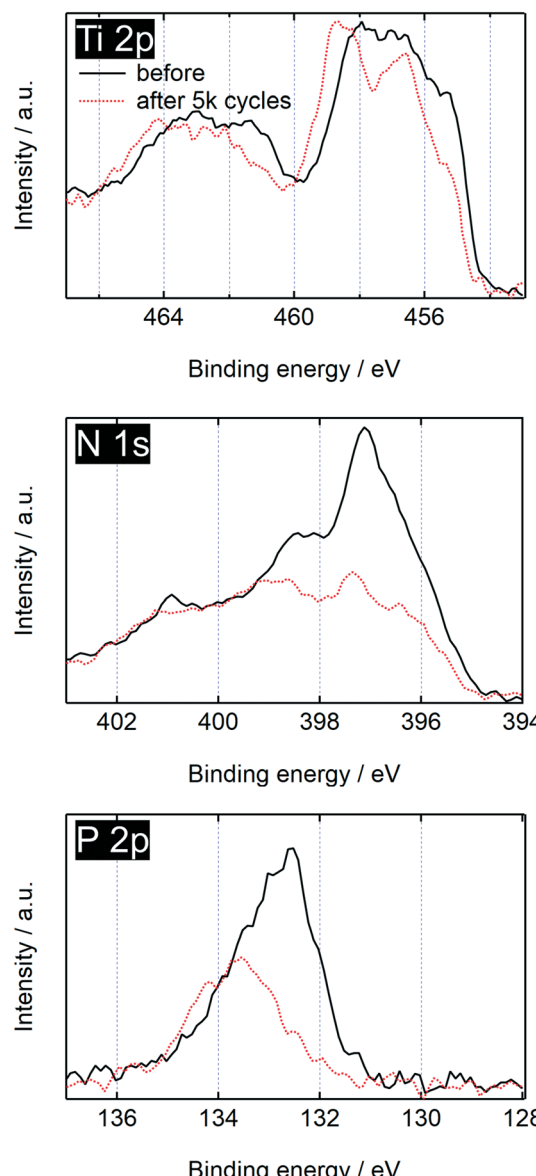


Fig. 6 XP $\text{Ti} 2p$, $\text{N} 1s$ and $\text{P} 2p$ spectra of $\text{TiO}_x\text{N}_y\text{P}_z$ catalyst before (solid curves) and after (dashed curves) 5000 potential cycles.

talyse ORR in acidic media. In addition to previously reported oxygen vacancy in the rutile, new P^{5+} -derived active sites were formed after optimisation of various synthesis conditions to successfully improve the activity with a catalyst loading of less than half of the previously reported phosphor-free TiO_xN_y catalysts. The source of the mass activity enhancement by more than double with P^{5+} -doping both in bulk and on surface, and the exact role of the phosphor; whether being an active site by itself or producing the site indirectly by forming titanium vacancy, etc., are to be investigated in the next step. However, the stabilization of the doped phosphor and nitrogen atoms in the surface rutile lattice at above 1.0 V was revealed necessary to use this catalyst without controlling the potential.

Conflicts of interest

There are no conflicts to declare.

Acknowledgements

The authors acknowledge Mr. Yusei Tsushima for his help with obtaining FE-SEM/TEM images. This study was partially supported by a Grant-in-Aid for Scientific Research (C), 17K06180, from the Ministry of Education, Culture, Sports, Science and Technology (MEXT) in Japan, a research grant from the Nippon Sheet Glass Foundation for Materials Science and Engineering, a research grant from the Yashima Environment Technology Foundation, Japan, a research grant from Suzuki Foundation, Japan and a research grant from Iketani Science and Technology Foundation, Japan. The XP spectra were acquired at the University of Tokyo, supported by the Nanotechnology Platform of MEXT in Japan.

Notes and references

- 1 C. E. Thomas, *Int. J. Hydrogen Energy*, 2009, **34**, 6005.
- 2 O. Gröger, H. A. Gasteiger and J. P. Suchsland, *J. Electrochem. Soc.*, 2015, **162**, A2605.
- 3 U. Eberle and R. von Helmolt, *Energy Environ. Sci.*, 2010, **3**, 689.
- 4 N. Konno, S. Mizuno, H. Nakaji and Y. Ishikawa, *SAE International Journal of Alternative Powertrains*, 2015, **4**, 123.
- 5 A. Kongkanand and M. F. Mathias, *J. Phys. Chem. Lett.*, 2016, **7**, 1127.
- 6 Fuel Cell Technologies Office Multi-Year Research, Development, and Demonstration Plan https://www.energy.gov/sites/prod/files/2017/05/f34/fcto_myrdd_fuel_cells.pdf.
- 7 U.S. Geological Survey, *Mineral commodity summaries 2018*, 2018, p. 124. <https://minerals.usgs.gov/minerals/pubs/mcs/2018/mcs2018.pdf>.
- 8 Organisation Internationale des Constructeurs d'Automobiles, 2018, 2017 Production statistics, <http://www.oica.net/category/production-statistics/2017-statistics/>.
- 9 E. Proietti, F. Jaouen, M. Lefèvre, N. Larouche, J. Tian, J. Herranz and J. P. Dodelet, *Nat. Commun.*, 2011, **2**, 416.
- 10 J. Shui, C. Chen, L. Grabstanowicz, D. Zhao and D. J. Liu, *Proc. Natl. Acad. Sci. U. S. A.*, 2015, **112**, 7650; Y. C. Wang, Y. J. Lai, L. Song, Z. Y. Zhou, J. G. Liu, Q. Wang, X. D. Yang, C. Chen, W. Shi, Y. P. Zheng, M. Rauf and S. G. Sun, *Angew. Chem., Int. Ed.*, 2015, **54**, 9907; S. H. Ahn, X. Yu and A. Manthiram, *Adv. Mater.*, 2017, **29**, 1606534; Q. Liu, X. Liu, L. Zheng and J. Shui, *Angew. Chem., Int. Ed.*, 2018, **57**, 1204.
- 11 R. Chenitz, U. I. Kramm, M. Lefèvre, V. Glibin, G. Zhang, S. Sun and J. P. Dodelet, *Energy Environ. Sci.*, 2018, **11**, 365.
- 12 M. Chisaka, in *Electrocatalysts for Low Temperature Fuel Cells: Fundamentals and Recent Trends*, ed. T. Maiyalagan and V. S. Saji, Wiley-VCH, Weinheim, 2017, p. 423.
- 13 Y. Liu, A. Ishihara, S. Mitsushima, N. Kamiya and K. Ota, *Electrochim. Solid-State Lett.*, 2005, **8**, A400; J. H. Kim, A. Ishihara, S. Mitsushima, N. Kamiya and K. Ota, *Electrochim. Acta*, 2007, **52**, 2492; A. Ishihara, S. Doi, S. Mitsushima and K. Ota, *Electrochim. Acta*, 2008, **53**, 5442; M. Chisaka, T. Iijima, T. Yaguchi and Y. Sakurai, *Electrochim. Acta*, 2011, **56**, 4581.
- 14 M. Chisaka, A. Ishihara, H. Morioka, T. Nagai, S. Yin, Y. Ohgi, K. Matsuzawa, S. Mitsushima and K. Ota, *ACS Omega*, 2017, **2**, 678.
- 15 L. M. Roen, C. H. Paik and T. D. Jarvi, *Electrochim. Solid-State Lett.*, 2004, **7**, A19.
- 16 M. Chisaka, Y. Ando and N. Itagaki, *J. Mater. Chem. A*, 2016, **4**, 2501; M. Chisaka, Y. Ando and H. Muramoto, *Electrochim. Acta*, 2015, **183**, 100.
- 17 M. Chisaka, Y. Ando, Y. Yamamoto and N. Itagaki, *Electrochim. Acta*, 2016, **214**, 165.
- 18 M. Chisaka, Y. Yamamoto, N. Itagaki and Y. Hattori, *ACS Appl. Energy Mater.*, 2018, **1**, 211.
- 19 M. Chisaka, *Phys. Chem. Chem. Phys.*, 2018, **20**, 15613.
- 20 Y. Furubayashi, T. Hitotsugi, Y. Yamamoto, K. Inaba, G. Kinoda, Y. Hirose, T. Shimada and T. Hasegawa, *Appl. Phys. Lett.*, 2005, **86**, 25101; X. Lü, X. Mou, J. Wu, D. Zhang, L. Zhang, F. Huang, F. Xu and S. Huang, *Adv. Funct. Mater.*, 2010, **20**, 509; D. S. Bhachu, S. Sathasivam, G. Sankar, D. O. Scanlon, G. Cibin, C. J. Carmalt, I. P. Parkin, G. W. Watson, S. M. Bawaked, A. Y. Obaid, S. Al-Thabaiti and S. N. Basahel, *Adv. Funct. Mater.*, 2014, **24**, 5075.
- 21 T. Hitotsugi, Y. Furubayashi, A. Ueda, K. Itabashi, K. Inaba, Y. Hirose, G. Kinoda, Y. Yamamoto, T. Shimada and T. Hasegawa, *Jpn. J. Appl. Phys.*, 2005, **44**, L1063; S. M. Bawaked, S. Sathasivam, D. S. Bhachu, N. Chadwick, A. Y. Obaid, S. Al-Thabaiti, S. N. Basahel, C. J. Carmalt and I. P. Parkin, *J. Mater. Chem. A*, 2014, **2**, 12849.
- 22 S. P. Madhusudanan, B. Gangaja, A. G. Shyla, A. S. Nair, S. V. Nair and D. Santhanagopalan, *ACS Sustainable Chem. Eng.*, 2017, **5**, 2393.
- 23 C. Sotelo-Vazquez, N. Noor, A. Kafizas, R. Quesada-Cabrera, D. O. Scanlon, A. Taylor, J. R. Durrant and I. P. Parkin, *Chem. Mater.*, 2015, **27**, 3234.
- 24 J. C. Yu, L. Zhang, Z. Zheng and J. Zhao, *Chem. Mater.*, 2003, **15**, 2280.
- 25 Q. Shi, D. Yang, Z. Jiang and J. Li, *J. Mol. Catal. B: Enzym.*, 2006, **43**, 44; L. Lin, W. Lin, J. L. Xie, Y. X. Zhu, B. Y. Zhao and Y. C. Xie, *Appl. Catal., B*, 2007, **75**, 52; Y. Xia, Y. Jiang, F. Li, M. Xia, B. Xue and Y. Li, *Appl. Surf. Sci.*, 2014, **289**, 306.
- 26 F. Li, Y. Jiang, M. Xia, M. Sun, B. Xue, D. Liu and X. Zhang, *J. Phys. Chem. C*, 2009, **113**, 18134.
- 27 H. Daimon and Y. Kurobe, *Catal. Today*, 2006, **111**, 182.
- 28 H. Daimon, O. Kitakami, O. Inagoya and A. Sakemoto, *Jpn. J. Appl. Phys.*, 1991, **30**, 282.
- 29 J. C. Parker and R. W. Siegel, *Appl. Phys. Lett.*, 1990, **57**, 943; X. H. Wang, J. G. Li, H. Kamiyama, M. Katada, N. Ohashi, Y. Moriyoshi and T. Ishigaki, *J. Am. Chem. Soc.*, 2005, **127**, 10982.
- 30 R. J. Betsch, H. L. Park and W. B. White, *Mater. Res. Bull.*, 1991, **26**, 613.
- 31 M. Chisaka, A. Ishihara, K. Suito, K. Ota and H. Muramoto, *Electrochim. Acta*, 2013, **88**, 697.

- 32 K. S. Robinson and P. M. A. Sherwood, *Surf. Interface Anal.*, 1984, **6**, 261.
- 33 N. C. Saha and H. G. Tompkins, *J. Appl. Phys.*, 1992, **72**, 3072.
- 34 J. Wang, W. Zhu, Y. Zhang and S. Liu, *J. Phys. Chem. C*, 2007, **111**, 1010; G. Yang, Z. Jiang, H. Shi, T. Xiao and Z. Yan, *J. Mater. Chem.*, 2010, **20**, 5301.
- 35 C. Rath, P. Mohanty, A. C. Pandey and N. C. Mishra, *J. Phys. D: Appl. Phys.*, 2009, **42**, 205101.
- 36 G. S. Shao, F. Y. Wang, T. Z. Ren, Y. Liu and Z. Y. Yuan, *Appl. Catal., B*, 2009, **92**, 61; G. S. Shao, T. Y. Ma, X. J. Zhang, T. Z. Ren and Z. Y. Yuan, *J. Mater. Sci.*, 2009, **44**, 6754.
- 37 L. Lin, R. Y. Zheng, J. L. Xie, Y. X. Zhu and Y. C. Xie, *Appl. Catal., B*, 2007, **76**, 196.
- 38 S. Baunack, S. Oswald and D. Scharnweber, *Surf. Interface Anal.*, 1998, **26**, 471.
- 39 F. M. Hossain, G. E. Murch, L. Sheppard and J. Nowotny, *Adv. Appl. Ceram.*, 2007, **106**, 95.
- 40 T. Norby, *MRS Bull.*, 2009, **34**, 923.
- 41 S. M. Wu, X. L. Liu, X. L. Lian, G. Tian, C. Janiak, Y. X. Zhang, Y. Lu, H. Z. Yu, J. Hu, H. Wei, H. Zhao, G. G. Chang, G. Van Tendeloo, L. Y. Wang, X. Y. Yang and B. L. Su, *Adv. Mater.*, 2018, **30**, 1802173.
- 42 P. Ruetschi, *J. Electrochem. Soc.*, 1984, **131**, 2737.
- 43 T. Zhai, L. Wan, S. Sun, Q. Chen, J. Sun, Q. Xia and H. Xia, *Adv. Mater.*, 2017, **29**, 1604167.
- 44 M. Abdullah, G. K. C. Low and R. W. Matthews, *J. Phys. Chem.*, 1990, **94**, 6820.
- 45 X. Chen, L. Liu, P. Y. Yu and S. S. Mao, *Science*, 2011, **331**, 746.
- 46 A. Ohma, K. Shinohara, A. Iiyama, T. Yoshida and A. Daimaru, *ECS Trans.*, 2011, **41**, 775.
- 47 C. A. Reiser, L. Bregoli, T. W. Patterson, J. S. Yi, J. D. Yang, M. L. Perry and T. D. A. Jarvi, *Electrochim. Solid-State Lett.*, 2005, **8**, A273.
- 48 U. Eberle and R. von Helmolt, *Energy Environ. Sci.*, 2012, **5**, 8780.
- 49 C. H. Choi, C. Baldizzone, J. P. Grote, A. K. Schuppert, F. Jaouen and K. J. J. Mayrhofer, *Angew. Chem., Ind. Ed.*, 2015, **54**, 12753; G. Zhang, R. Chenitz, M. Lefèvre, S. Sun and J. P. Dodelet, *Nano Energy*, 2016, **29**, 111; J. Y. Choi, L. Yang, T. Kishimoto, X. Fu, S. Ye, Z. Chen and D. Banham, *Energy Environ. Sci.*, 2017, **10**, 296.
- 50 X. Chen, X. Wang, Y. Hou, J. Huang, L. Wu and X. Fu, *J. Catal.*, 2008, **255**, 59.
- 51 G. Li, Y. Li, H. Liu, Y. Guo, Y. Li and D. Zhu, *Chem. Commun.*, 2010, **46**, 3256; Y. Li, L. Xu, H. Liu and Y. Li, *Chem. Soc. Rev.*, 2014, **43**, 2572; Z. Jia, Y. Li, Z. Zuo, H. Liu, C. Huang and Y. Li, *Acc. Chem. Res.*, 2017, **50**, 2470; C. Huang, Y. Li, N. Wang, Y. Xue, Z. Zuo, H. Liu and Y. Li, *Chem. Rev.*, 2018, **118**, 7744.
- 52 N. Yang, Y. Liu, H. Wen, Z. Tang, H. Zhao, Y. Li and D. Wang, *ACS Nano*, 2013, **7**, 1504.